Journal of Power Sources 196 (2011) 2994–3002

Contents lists available at ScienceDirect

Journal of Power Sources

journal homepage: www.elsevier.com/locate/jpowsour

CO electrooxidation study on Pt and Pt–Ru in H_3PO_4 using MEA with PBI–H_3PO_4 membrane

A.D. Modestov*, M.R. Tarasevich, A.Y. Leykin

A.N. Frumkin Institute of Physical Chemistry and Electrochemistry, Russian Academy of Sciences, Leninsky Prosp. 31, Moscow 119991, Russia

ARTICLE INFO

Article history:
Received 20 September 2010
Received in revised form
13 November 2010
Accepted 18 November 2010
Available online 24 November 2010

Keywords:
PBI
PEMFC
CO electrooxidation
CO tolerance
Pt
Pt–Ru

ABSTRACT

CO electrooxidation on Pt and Pt–Ru in H_3PO_4 was studied in the temperature range 120–180 °C using CO–N_2–H_2O gas mixtures of controlled composition. On Pt and Pt–Ru the voltammetry curves exhibited Tafel behavior in a wide potential range with a slope of 80–100 mV per decade. Replacement of Pt with Pt–Ru on the anode resulted mainly in a shift of CO electrooxidation voltammetry curves by approx. −0.3 V. Reaction order in respect to water vapor pressure was found close to unity with both electrocatalysts. Reaction order in respect to CO partial pressure was found negative, close to zero. Values of apparent activation energy of CO electrooxidation on these electrocatalysts were nearly equal, $E_{a\,app} = 110 \pm 15$ kJ mol^{-1}. The results were interpreted within the framework of Langmuir–Hinshelwood mechanism. An equation, which describes the observed features of CO electrooxidation on Pt and Pt-Ru, was suggested. Comparing results of the present study with results of earlier studies of CO tolerance of Pt and Pt–Ru electrocatalysts, it was concluded that CO electrooxidation can hardly play a significant role in CO tolerance of PEM FC with PBI–PA membranes.

1. Introduction

CO electrooxidation on Pt based electrocatalysts is an important process at least for two reasons. Firstly, hydrogen oxidation anodes of polymer electrolyte membrane fuel cells (PEM FC) are deactivated in the presence of CO in hydrogen (CO poisoning). CO is an unavoidable impurity in hydrogen produced by steam reforming of hydrocarbons. In PEM FC operational at temperatures below 80 °C surface of Pt hydrogen oxidation catalyst is almost blocked by adsorbed CO even in CO presence in fuel at 10 ppm level [1–3]. CO tolerance of Pt based hydrogen oxidation electrocatalysts is often attributed to removal of adsorbed CO by electrooxidation. Secondly, adsorbed CO is an intermediate species produced in electrooxidation of methanol, ethanol and some other hydrocarbon fuels that could be used in PEM FC [4]. Elevation of the operational temperature of FC improves CO tolerance of hydrogen–air FC and increases the rate of methanol (ethanol) electrooxidation. The use of phosphoric acid fuel cells (PAFC) and PEM FC with the membrane of phosphoric acid (PA) doped polybenzimidazole (PBI) increased operational temperature range of FC up to 160–200 °C [5–15]. As a result, CO tolerance of these FCs reached few percent. Methanol [16,17], ethanol [18,19], and formic acid [20] were tried as a fuel for PEM FC with PBI–PA membranes.

CO tolerance of Pt based anode catalysts can be improved by alloying platinum with some noble and non-noble metals. Pt–Ru is one of the most CO tolerant platinum based hydrogen oxidation catalysts [21,22]. The increase of CO tolerance by addition of the second component to Pt is often ascribed to the increased rate of CO electrooxidation, which temporarily frees portion of the sites at the catalyst surface for hydrogen oxidation reaction [23]. CO electrooxidation on Pt based catalysts proceeds via Langmuir–Hinshelwood mechanism [23–38], which involves reaction of adsorbed species. The mechanism was proposed by Langmuir in 1922 to account for kinetics of Pt catalyzed CO oxidation [39].

Standard equilibrium potential of CO electrooxidation is approx. −0.1 V vs. hydrogen reference [1]. The mechanism of CO electrooxidation involves the following consecutive reactions, which occur at the catalyst surface [31,35,36]:

$$CO + [*] \rightarrow CO_{ads} \quad (1)$$

$$H_2O + [*] \rightarrow OH_{ads} + H^+ + e^- \quad (2)$$

$$CO_{ads} + OH_{ads} \rightarrow COOH_{ads} \quad (3)$$

$$COOH_{ads} \rightarrow CO_2 + H^+ + e^- \quad (4)$$

Here [*] stands for the vacant site at the catalyst surface. Electrochemical reaction (2) generates adsorbed active oxygen containing species, which are designated by OH_{ads}. Reaction (3) between adsorbed reactants can be a rate-determining stage under certain conditions [31,35,36,40]. According to bifunctional mechanism of

* Corresponding author. Tel.: +7 495 9522387; fax: +7 495 9525308.
E-mail address: modestov@elchem.ac.ru (A.D. Modestov).

0378-7753/$ – see front matter © 2010 Elsevier B.V. All rights reserved.
doi:10.1016/j.jpowsour.2010.11.091

the enhanced CO tolerance of Pt–Ru (and some other Pt alloys) hydrogen oxidation electrocatalysts [23], Ru (second metal component) surface atoms provide active oxygen containing species (OH_{ads}), which are not available on pure Pt in a practically important for FC operation potential range. Catalytic activity of Ru in CO oxidation reaction is rather poor [41] primarily because CO does not adsorb on oxidized Ru. Therefore, on Pt–Ru, reaction (3) is supposed to occur on Pt surface atoms.

According to the alternative mechanism of CO tolerance of platinum alloy hydrogen oxidation catalysts, alloying with the second metal modifies electronic properties of the Pt based catalyst so that CO adsorption level is reduced without involvement of CO electrooxidation reaction [22,42–49]. The increase of PAFC CO tolerance by use of Pt–Ru alloy in place of pure Pt on the anode was observed in [42,50]. At 180 °C methanol electrooxidation activity of Pt–Ru in PA was found superior to Pt [51]. The use of PBI–PA membranes to increase operational temperature of PEM FC was proposed in [52,53].

The electrolyte held in the pores of the catalyst layers (CLs) of PEM FC with PBI–PA membranes are pure PA or PBI doped with PA. Incorporation of PA molecules in the PBI framework does not alter essentially Grottgus mechanism of protonic conductivity in concentrated PA [54–57]. Concentration of phosphoric acid in CLs of PAFC or PEM FC with PBI–PA membranes is ~100% [58,59]. The only source of surface OH_{ads} species for CO electrooxidation is oxidation of water molecules by reaction (2). H_2O concentration in PA contained in the pores of the CLs of the MEA with PBI–PA membrane can be controlled by the reactant gas humidification. Data on equilibrium water vapor pressure over PA at elevated temperatures was reported [60,61]. Due to exceptionally high rate of hydrogen oxidation/reduction on Pt, the opposite gas diffusion electrode (GDE) of the MEA supplied with hydrogen can be used as both a counter and a reference electrodes of the cell.

CO tolerance of Pt and Pt–Ru hydrogen oxidation catalysts was compared at 140–180 °C using MEA with PBI–PA membrane [59]. The goal of the present work was to investigate the main features of the CO electrooxidation on Pt and Pt–Ru catalysts in the operational temperature range of PEMFC with PBI–PA membrane in order to clarify the role of CO electrooxidation reaction in CO tolerance of these catalysts.

2. Experimental

MEA preparation protocol was described elsewhere [59,62,63]. Briefly, small MEAs of 6 cm^2 active area were used in order to match with the output of potentiostat/galvanostat PARSTAT 2273 (Princeton Applied Research). PARSTAT 2273 was also employed in EIS measurements that were used to detect the cell resistance. Arbin FCTS-50 test station was employed to prepare gas mixtures of the required composition and to control the cell temperature. Most of the experiments were conducted in a cell driven mode. GDEs were manufactured by spray coating catalyst ink on gas diffusion layers, which were Sigracet 10DC (SGL Group). Pt or Pt–Ru (Johnson-Matthey, HiSPEC 9000 or HiSPEC 10000, 60% platinum group metal supported on carbon) were used on the working electrode. Counter electrodes in all cases contained Pt catalyst. Platinum group metal loading at all electrodes was within 1.2–1.5 mg cm^{-2} range. Catalyst inks were prepared using Nafion 5% solution (DuPont). Nafion was used as a binder only to preserve integrity of the catalyst layers during MEA fabrication. Dry Nafion concentration in the CLs was 3% relative to carbon support. The electrolyte in the CLs of the GDEs was phosphoric acid. The films of poly[2,2′-diphenyloxide-5,5′-bibenzimidazole] (PBI) were supplied by the National Innovation Company "New Energy Projects":

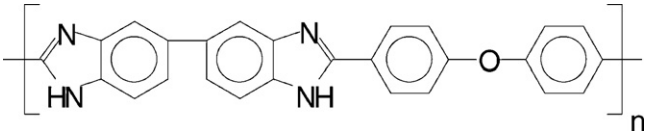

Details of the PBI synthesis and film casting were reported elsewhere [64,65]. The 26–30 μm thick PBI films were doped in 85% H_3PO_4 (PA-ACS-ISO Panreac) in closed vessel at 110–130 °C for at least 70 h. Two doped PBI films were stacked to produce ~100 μm thick membrane. The membrane, GDEs, and attached polytetrafluoroethylene gaskets were assembled by hot pressing between plates of the Carver automatic press at 130 °C for 15 min. As a result of hot pressing, fraction of PA, initially kept in the membrane, was squeezed out into the catalyst layers. For testing the MEA was placed in a test cell (Arbin). Gas mixtures of different compositions were prepared using mass flow controllers and gas humidifiers of the test station. Hydrogen 99.999%, nitrogen 99.999%, oxygen 99.999% and carbon monoxide 99.8% were used. The exhaust lines of the test cell were open to the atmosphere. Water vapor pressure (P_W) in the gas mixtures was controlled by gas humidification. P_W values were calculated using data on temperature dependence of water saturated vapor pressure [66]. Concentrations of CO and N_2 in gas mixtures were tuned using respective mass flow controllers taking into account ambient pressure in the test cell (1 bar) and a chosen P_W. Concentrations of components in the gas phase are indicated in units of partial pressure (bar). Within the accuracy range of our experiments, values of partial pressure numerically coincide with the volume fractions of the components. In CO electrooxidation studies the counter electrode was supplied with hydrogen. Gases, which were supplied to the opposite electrodes of the MEA, were humidified to reach the same P_W. Hydrogen, water vapor, carbon monoxide, and oxygen stoichiometry numbers were at least 10 to ensure uniformity of current density distribution over the electrode surface.

The EIS measurements were staged at open circuit voltage in 0.1 Hz–20 kHz frequency domain, using sinusoidal voltage ripple of 20 mV amplitude. 0.2 mV s^{-1} voltage scan rate was used in voltammetry measurements. In our earlier studies [59] the overpotential of neat hydrogen oxidation/reduction was found negligible compared to the overpotential of CO electrooxidation. Therefore, the potential of the counter electrode flushed by neat hydrogen virtually coincided with the potential of the reversible hydrogen electrode. Corrections were applied to account for the Nernstian shift of the hydrogen electrode potential caused by the hydrogen partial pressure reduction with humidification. The electrode potential readings (E) are given vs. RHE.

3. Results

3.1. CO electrooxidation at 180 °C

Representative voltammetry curves of CO electrooxidation on Pt and Pt–Ru at 180 °C are shown in Tafel coordinates in Figs. 1 and 2, respectively. Potential readings were corrected for ohmic losses using data of the EIS measurements. The CO electrooxidation curves shown in Fig. 1 were measured using gas mixtures of different humidity. P_W was varied within the range 0.054–0.38 bar. CO partial pressure (P_{CO}) was kept within the range 0.17–0.22 bar. As it will be shown below, in this P_{CO} domain, current density (i) of CO electrooxidation is virtually independent of P_{CO}. The curves, shown in Fig. 1, prove the increase of CO electrooxidation rate with the increase of P_W. Tafel curves of CO electrooxidation on Pt–Ru at 180 °C are shown in Fig. 2. In this case, CO electrooxidation was performed at fixed P_W = 0.47 bar, while P_{CO} was varied. In all our experiments Tafel type of potential dependence of CO oxidation currents was observed in a relatively wide potential range. In the

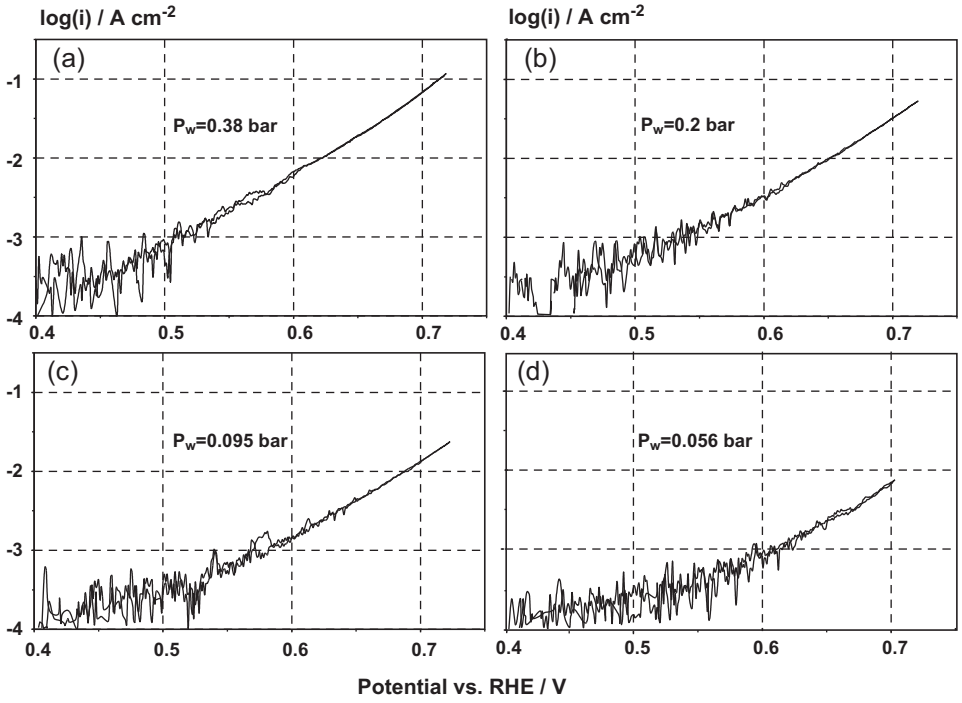

Fig. 1. Representative voltammetry curves of CO electrooxidation on Pt at 180 °C. P_W values are indicated on the respective panels. P_{CO} was kept within the range 0.17–0.22.

Tafel regions the slope of CO electrooxidation curves, shown in Figs. 1 and 2, was within the range 90–100 mV per decade, both on Pt and Pt–Ru. The curves deviated from Tafel behavior at relatively low CO oxidation overvoltages, when current densities were below ~0.3 mA cm^{-2}. It apparently happened when CO oxidation currents became comparable with the current contributions arising from hydrogen pumping and hydrogen crossover processes. At low P_{CO}, e.g. in Fig. 2(a)–(d), a limiting current of CO electrooxidation was observed at high potentials. Dependence of the limiting current density on P_{CO} is shown in Fig. 3(a). The voltammetry curves of CO electrooxidation on Pt–Ru at 180 °C, P_W = 0.47 bar were used to plot this graph. The linear dependence of the limiting current density on P_{CO} helps to ascribe the cause of the limiting current to CO transport limitations in the gas diffusion electrode. To check the concept, performance curves of the MEA with PBI–PA membrane and Pt catalyst at both electrodes were measured at 180 °C using dry neat hydrogen as a fuel and dry O_2–N_2 mixtures of various composition as an oxidant (the curves are not shown). In this case at low oxygen concentration limiting currents were observed. Apparently, the cell performance in these cases was controlled by oxygen mass transport through the cathode GDE [67,68]. Dependence of oxygen mass transport limited current on oxygen partial pressure in the oxidant measured with this MEA at 180 °C is shown in Fig. 3(b). The slope of the dependence of mass transport limited oxygen reduction current on oxygen partial pressure is ~8 A cm^{-2} bar^{-1}, that is higher by a factor of ~1.3 than the slope of the dependence of CO electrooxidation limited current on P_{CO}, ~6.3 A cm^{-2} bar^{-1}, Fig. 3(a). Four electron reduction of O_2 molecule requires twice more electrons than CO electrooxidation, therefore the slope of the dependence in this case is supposed to be twice higher than the slope measured in case of CO electrooxidation. The diffusivities of CO and O_2 molecules are nearly equal [66]. Taking all that into account, we conclude that our measurements of mass transport limited currents of CO oxidation and of mass transport limited currents of O_2 reduction with the PBI–PA based MEA are in qualitative agreement. Therefore, the potential independent currents of CO electrooxidation observed at relatively low P_{CO} and high overvoltages arise from CO mass transport limitations in GDE rather than from a chemical reaction.

Dependence of CO electrooxidation current on P_{CO} in the anode gas feed is shown in Fig. 4. Measurements with MEAs, containing Pt or Pt–Ru on the anode, were staged at P_W = 0.47 bar. CO electrooxidation was studied in the P_{CO} range between 0.005 bar and 0.53 bar. Current readings were taken at fixed potentials falling within the Tafel regions of the corresponding voltammetry curves. Solid circles in Fig. 4 show i–P_{CO} dependence measured on Pt. Current density readings were taken at E = 0.55 V. i–P_{CO} dependence on Pt–Ru is shown in Fig. 4 by open circles. In this case current readings were taken at E = 0.3 V. As it follows from the data shown in Fig. 4, the i–P_{CO} dependencies measured on Pt and Pt–Ru follow the same trend. CO electrooxidation rate slightly increases with the decrease of P_{CO} at relatively high P_{CO}, from 0.53 bar to ~0.1 bar, with the steeper increase of CO electrooxidation rate with P_{CO} decrease below ~0.1 bar.

Dependence of CO electrooxidation rate on P_W at fixed CO concentration at 180 °C on Pt and Pt–Ru is shown in Fig. 5. The data points were extracted from the Tafel regions of the corresponding voltammetry curves. P_W was changed within 0.39–0.04 bar region. The results of experiments with Pt and Pt–Ru are shown in Fig. 5(a) and (b) respectively, using log–log coordinates. The linear dependence of CO electrooxidation rate on P_W both on Pt and Pt–Ru with the slope 1 ± 0.1 in this set of coordinates indicates that CO electrooxidation in both cases is of the first order with respect to P_W.

Measurements at 180 °C were complicated by the decline of the electrochemical activity of Pt–Ru. Typically, after about 10 h of potential cycling within 0.2–0.5 V region, CO electrooxidation current on Pt–Ru decreased approximately by a factor of 2. Degradation of Pt–Ru in PA at 180 °C caused by selective dissolution of Ru at high potentials was observed earlier in studies of methanol electrooxidation [51]. For this reason, the more detailed study of CO electrooxidation was staged at 140 °C. At this temperature the life time of Pt–Ru under above indicated conditions increased at least tenfold.

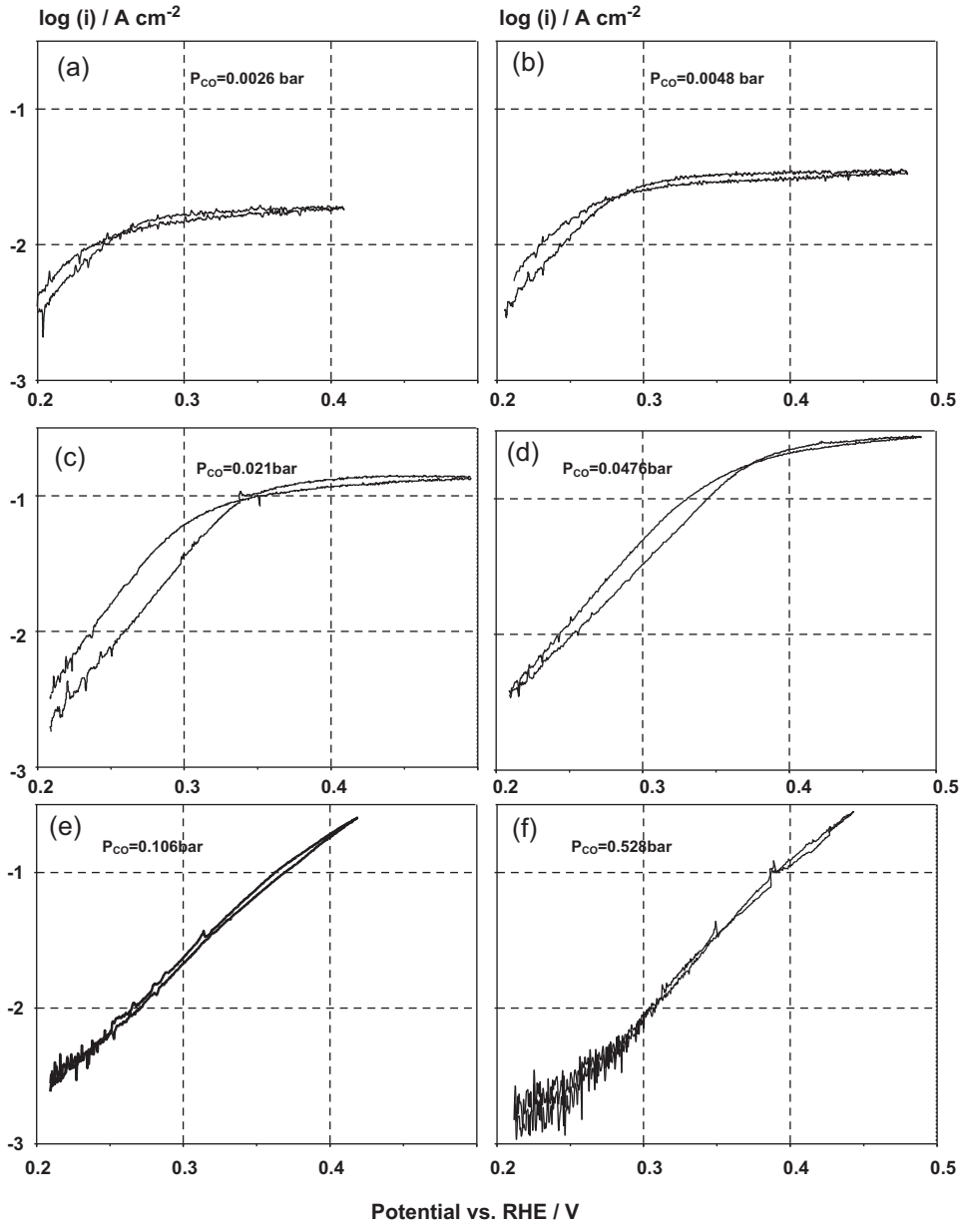

Fig. 2. Representative voltammetry curves of CO electrooxidation on Pt–Ru at 180 °C, P_W = 0.47 bar. P_{CO} values are indicated on the respective panels.

3.2. CO electrooxidation at 140 °C

Dependence of CO electrooxidation rate on decimal logarithm of P_{CO} is shown in Fig. 6. Measurements were staged using MEAs with Pt or Pt–Ru catalysts in CLs of the working electrode. CO oxidation current density readings were taken at fixed potentials within the Tafel region of the respective voltammetry curves (not shown). Compared to the experiments at 180 °C, CO electrooxidation at 140 °C was studied in a wider P_{CO} range 0.95–0.0018 bar. The curves of the dependence shown in Fig. 6 follow the trend that was observed with these catalysts at 180 °C, Fig. 4. At high P_{CO}, ~0.95–0.1 bar, CO electrooxidation rate slightly decreases with the increase of P_{CO}. However, at low P_{CO}, ~0.0018–0.03 bar, CO electrooxidation current decreases nearly linearly with the increase of the decimal logarithm of P_{CO}. Therefore, the CO electrooxidation reaction order in respect to P_{CO} (m) is negative and dependent on P_{CO}. The CO electrooxidation order in respect to P_{CO}, averaged over the whole range of P_{CO}, 0.95–0.0018 bar, is $m \sim -0.01$ both on Pt and Pt–Ru.

Dependence of CO electrooxidation rate on P_W measured on Pt and Pt–Ru at 140 °C, is shown in Fig. 7(a) and (b), respectively. The measurements were performed at low P_{CO}, falling within the region of linear dependence of CO electrooxidation current on log(P_{CO}), and at high P_{CO}. The results are presented as log–log graph. The slope of the curves in all cases is 1.05 ± 0.1. Therefore CO electrooxidation reaction order in respect to P_W both on Pt and PtRu at 140 °C is close to unity in all cases.

3.3. Temperature dependence of CO electrooxidation rate

Tafel curves of CO electrooxidation measured at 120, 140, 160 and 180 °C on Pt and Pt–Ru are shown in Fig. 8(a) and (b), respectively. Gas mixtures of constant P_{CO} = 0.07 bar were used in these experiments. To keep water concentration in the PA constant in this set of experiments, gas mixtures were supplied to the cell at the same value of relative humidity, RH = $P_W/P_{W\,sat}$ = 0.025. Here $P_{W\,sat}$ stands for the saturation pressure of water vapors at the cell temperature. Fractions of curves in the region of low values

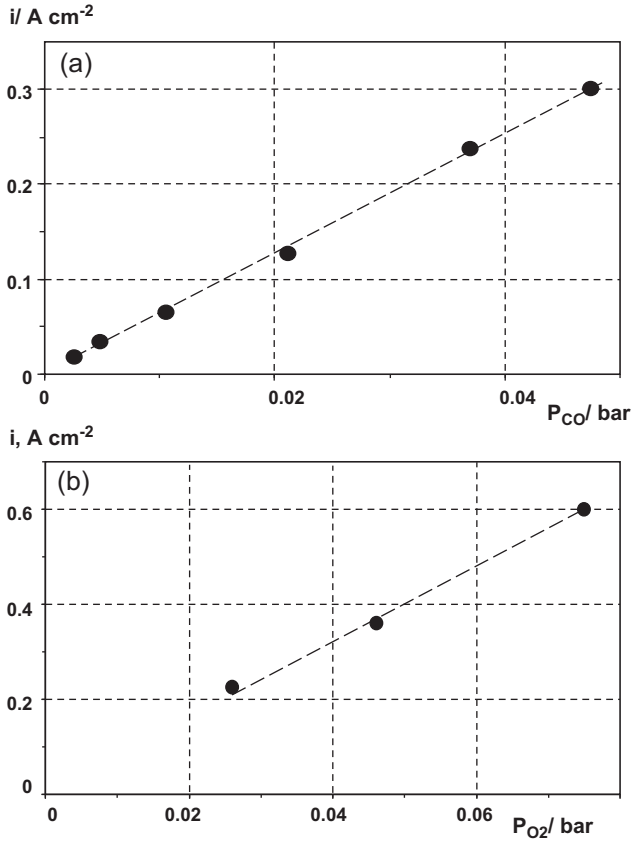

Fig. 3. Mass transport limited currents measured with MEA with PA–PBI membrane at180 °C. (a) Dependence of CO electrooxidation mass transport limited current on P_{CO}, Pt–Ru, P_W = 0.47 bar; (b) dependence of oxygen mass transport limited current on oxygen concentration in the oxidant feed, cathode (anode) was supplied with O_2–N_2 mixture (neat H_2).

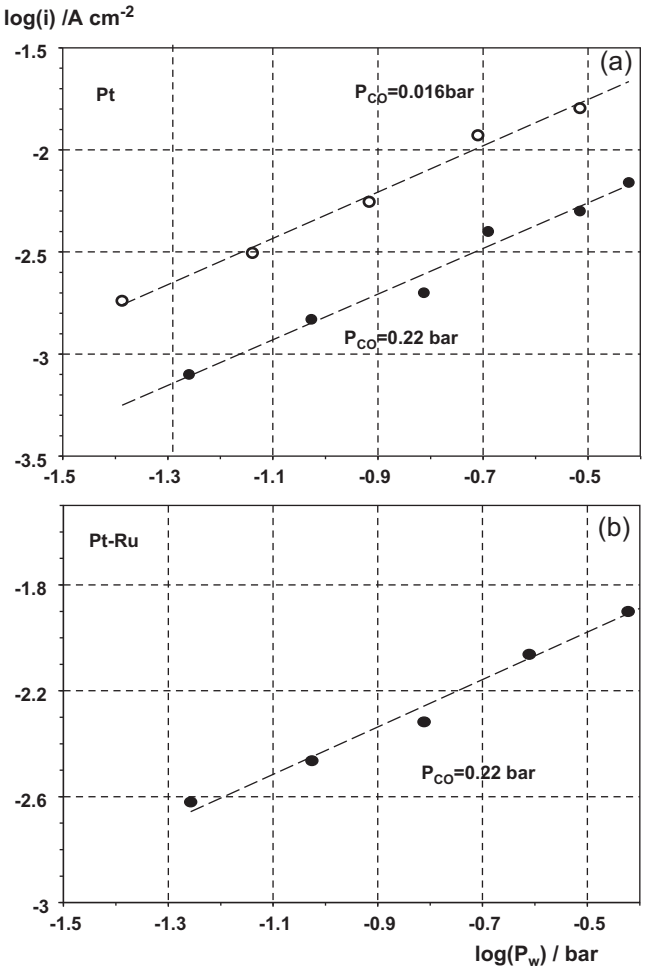

Fig. 5. Dependence of CO electrooxidation currents on P_W at 180 °C: (a) Pt, E = 0.6 V; (b) Pt–Ru, E = 0.4 V. P_{CO} values are indicated at the curves.

of CO electrooxidation currents, below ~0.3 mA cm^{-2}, were omitted due to high scatter of data points, that is caused by low signal to noise ratio. The slope values in Tafel regions for all curves shown in Fig. 8(a) and (b) fall in the range 80–100 mV per decade. Deviation from the linear dependence log(i) vs. E observed in Fig. 8(b) at i higher than 0.1 A cm^{-2} can be ascribed to mass transport limitations, that influence voltammetry at high current densities. The effect of temperature on CO electrooxidation rate on Pt and Pt–Ru is shown in Fig. 8(c) in Arrhenius coordinates. The data points were taken from the voltammetry curves shown in Fig. 8(a) and (b). To plot the dependence, the current density readings were taken at E = 0.7 V with Pt, and at E = 0.4 V with Pt–Ru. CO electrooxidation currents measured at these potentials on Pt and Pt–Ru are nearly equal. It suggests that the Tafel regions of CO electrooxidation curves measured on Pt and Pt–Ru are separated on potential axis by a gap of ~0.3 V. The slope value of the linear fit of data points is translated into the value of apparent activation energy [69] of CO

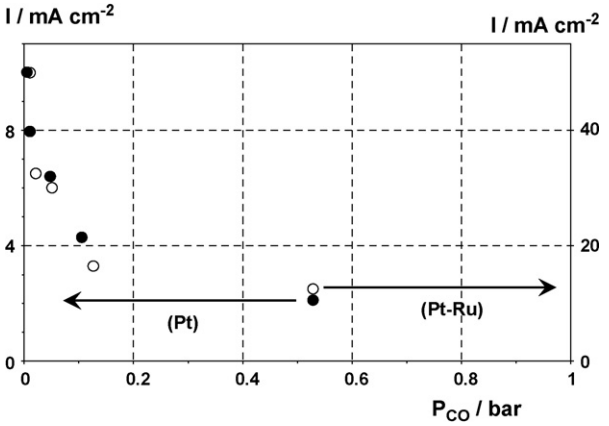

Fig. 4. Dependence of CO electrooxidation currents on P_{CO} at 180 °C, P_W = 0.47 bar: ● – Pt at E = 0.55 V; ○ – Pt–Ru at E = 0.3 V.

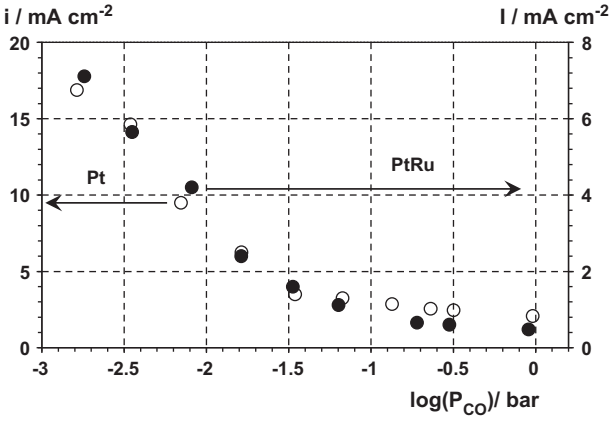

Fig. 6. Dependence of CO electrooxidation currents on CO partial pressure at 140 °C: ● – Pt–Ru, E = 0.36 V, P_W = 0.041 bar; ○ – Pt, E = 0.7 V, P_W = 0.094 bar.

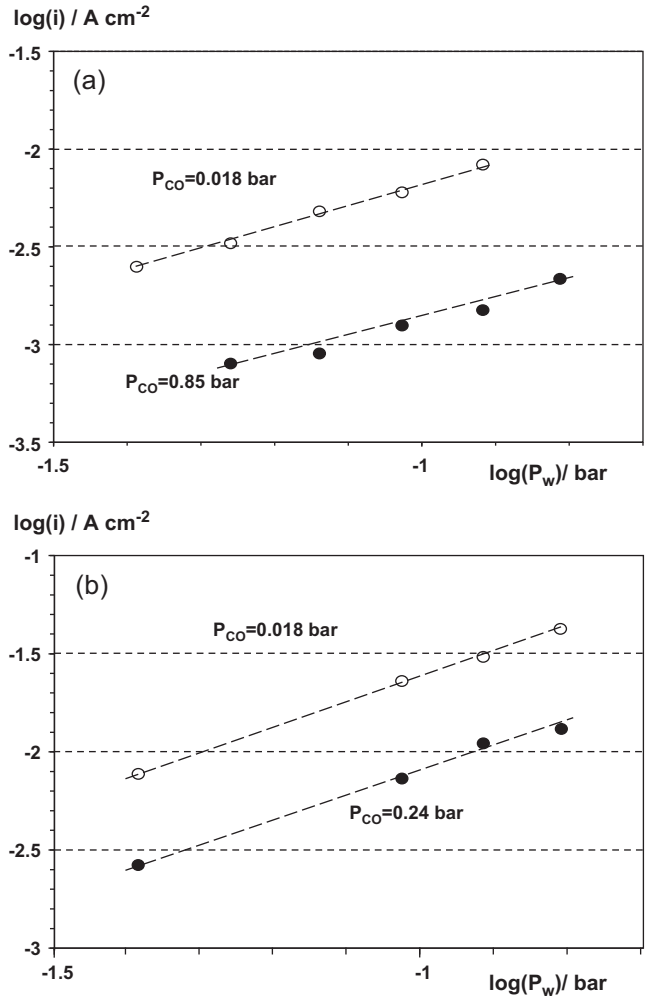

Fig. 7. Dependence of CO electrooxidation currents on P_W at 140 °C: (a) Pt, $E = 0.7$ V; (b) Pt–Ru, $E = 0.4$ V. P_{CO} values are indicated at the curves.

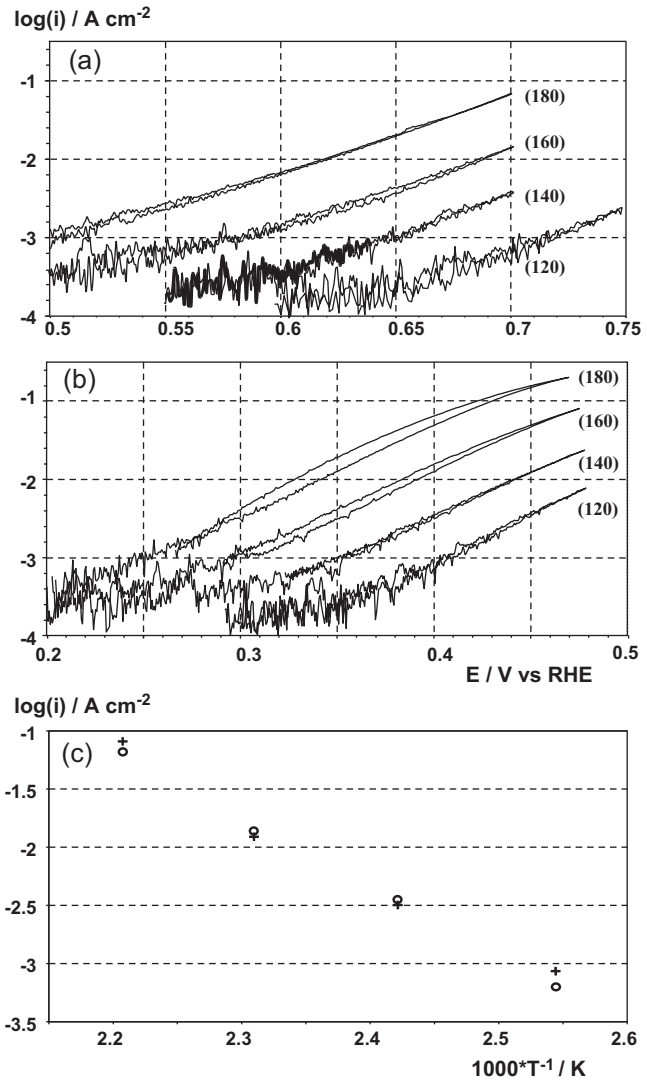

Fig. 8. Dependence of CO electrooxidation rate on temperature: (a) Pt; (b) Pt–Ru. Temperature readings are indicated at the curves, relative humidity of gases RH = 0.025 at all temperatures, $P_{CO} = 0.07$ bar and (c) Temperature dependence of CO electrooxidation currents measured on Pt and Pt–Ru at fixed potentials: ○ – Pt, at $E = 0.7$ V; + – Pt–Ru, at $E = 0.4$ V. Current density on Pt–Ru at 180 °C, $E = 0.4$ V was determined by extrapolation of the Tafel region. Current density readings were averaged between forward and backward potentials scans.

electrooxidation, $E_{a\,app} = 110 \pm 15$ kJ mol^{-1} both for Pt and Pt–Ru. Agreement between the values of $E_{a\,app}$, determined with these catalysts, suggests that there is no substantial difference in the reaction mechanisms of CO electrooxidation on Pt and Pt–Ru.

4. Discussion

Results of this study of CO electrooxidation on Pt and Pt–Ru can be explained within the framework of the Langmuir–Hinshelwood mechanism presented by the reaction sequence (1)–(4). Values of the slope of Tafel plots of CO electrooxidation voltammetry, ~80–100 mV per decade, Figs. 1, 2 and 8, are close to the value of 2.303 RT/F, which equals to 78 mV per decade at 120 °C, 82 mV per decade at 140 °C, 86 mV per decade at 160 °C, and 90 mV per decade at 180 °C. The Tafel slope values suggest that the EC mechanism of the overall process might include fast reversible one electron electrochemical step. Similarity of CO electrooxidation rate dependencies on E, P_{CO} and P_W, which were measured with Pt and Pt–Ru, attracts attention. As follows from Figs. 1, 2, 4–8, the use of Pt–Ru in place of Pt results mainly in a shift of the CO electrooxidation voltammetry curves by ~0.3 V along potential axis in negative direction. Low negative value of reaction order in respect to P_{CO}, $m \sim -0.01$, coupled with close to unity reaction order in respect to P_W, suggests that under the experimental conditions, electrocatalyst surface coverage by CO (θ_{CO}) approaches unity, while active oxygen containing species are formed at the scarce unoccupied by CO sites at the catalyst surface. According to [70], at 148 °C the increase of CO partial pressure in the gas phase from 0.005 bar to 1 bar results in the increase of CO coverage on Pt electrode in 96% PA from about 0.5 to 0.987. One can assume that under the experimental conditions the change of P_{CO} alters θ_{CO} according to CO adsorption isotherm, maintaining θ_{CO} close to unity. In this case, relatively small change of θ_{CO}, caused by change of P_{CO}, might result in a dramatic change of a number of sites available for the formation of active oxygen containing species, that is proportional to $(1 - \theta_{CO})$. The rate of the chemical step (3) by the mean-field approximation model can be expressed by the equation:

$$r = k \times \theta_{CO} \times \theta_{OH} \quad (5)$$

where θ_{OH} stands for the catalyst surface coverage by the active oxygen containing species OH_{ads}. In the following, as long as mass transfer limitations are not reached, θ_{CO} is supposed to be potential independent and slow changing with P_{CO}. With reasonable accuracy this factor in Eq. (5) can be considered constant.

Taking into account the values of the voltammetry slope in Tafel regions, low, negative reaction order in respect to P_{CO}, and close to unity reaction order in respect to $P_{W,}$ the following simplified EC mechanism of CO oxidation can be suggested. It includes fast reversible reaction of CO adsorption, Eq. (1); fast reversible electrochemical step of water oxidation at the unoccupied by CO sites only, Eq. (2); rate-determining step of chemical reaction of adsorbed CO_{ads} with OH_{ads} species, Eq. (3); and fast irreversible electrochemical reaction, Eq. (4), which doubles the current density value. CO adsorption on Pt was shown to follow Temkin isotherm in hot phosphoric acid [70–72]. For θ_{CO} changing within the range approximately 0.2–0.8, Temkin adsorption isotherm can be approximated by the logarithmic dependence of θ_{CO} on P_{CO}, where c and β stand for the isotherm parameters [73,74]:

$$\theta_{CO} = c + \beta \quad \log(P_{CO}) \tag{6}$$

Fast reversible electrochemical oxidation of water molecules on Pt surface is presumed to proceed exclusively at the unoccupied by CO sites. The only source of OH_{ads} species is one electron oxidation of water dissolved in PA. Water concentration $[H_2O]$ in PA in equilibrium with humidified gas can be expressed by Henry equation [60]:

$$[H_2O] = h P_W \tag{7}$$

where h stands for the Henry constant. Reaction (2) is assumed to be fast, reversible and close to equilibrium. Therefore, OH_{ads} surface coverage, which is supposed to be very small, $\Theta_{OH} \ll 1$, can be expressed by the Nernst equation:

$$\begin{aligned}\theta_{OH} &= (1 - \theta_{CO} - \theta_{OH}) h P_W [H^+]^{-1} \exp[(E - E^0)F/RT] \\ &\sim (1 - \theta_{CO}) h P_W [H^+]^{-1} \exp[(E - E^0)F/RT]\end{aligned} \tag{8}$$

Here E^0 stands for the standard electrode potential of reaction (2). Concentration of protons in 100% PA is supposed to be of the order of PA concentration, virtually independent of the composition of the gas phase. Substituting Eqs. (6–8) into Eq. (5) we arrive at the equation, which places together the basic parameters of our experiments:

$$i = 2Fk[c + \beta \quad \log(P_{CO})] h [H^+]^{-1} [1 - c - \beta \quad \log(P_{CO})] P_W \times \exp[(E - E^0)F/RT] \tag{9a}$$

$$(E - E^0) = -2.303 \frac{RT}{F} \quad \log(K) + 2.303 \frac{RT}{F} \quad \log(i) \tag{9b}$$

$$\text{where } K = 2Fk[c + \beta \quad \log(P_{CO})] h [H^+]^{-1} [1 - c - \beta \quad \log(P_{CO})] P_W \tag{9c}$$

Eq. (9b) is of the form of Tafel equation. However, it is important to underline, that E^0 in Eqs. (9a) and (9b) stand for the standard equilibrium potential of the water oxidation reaction (2), but not for the equilibrium potential of CO electrooxidation reaction:

$$CO + H_2O \rightarrow CO_2 + 2H^+ + 2e^- \tag{10}$$

Eq. (2) actually describes formation of the surface oxide on the electrode surface. Therefore, E^0 depends strongly on the nature of the catalyst metal. In acidic aqueous electrolytes at 60 °C standard potential of reversible formation of surface oxide on Pt was found close to 1.0 V [69].

Eqs. (9a) and (9b) agree with our experimental data on dependence of CO oxidation current on E, P_W, and P_{CO}, as long as the mass transfer hindrance does not play a role. According to Eq. (9b) the slope of Tafel type dependence of CO oxidation current on potential is $2.303\,RT/F$ per decade. Under fixed E and P_{CO}, CO oxidation current is expected to be of the first order in respect to water vapor pressure. This agrees well with the experimental evidence presented in Figs. 5 and 7. Under conditions when CO adsorption follows the logarithmic isotherm, expressed by Eq. (6), CO oxidation current is expected to decrease linearly with the increase of $\log(P_{CO})$. The trend is caused by the decrease of a number of sites available for the water oxidation reaction, Eq. (2), with the increase of P_{CO}. The linear decrease of CO oxidation current with the increase of $\log(P_{CO})$ indeed takes place at $P_{CO} < 10^{-1.5} \approx 0.03$ bar on both electrocatalysts, Fig. 6. The deviation from the linear dependence, which occurs at $P_{CO} > 10^{-1.5}$ bar in Figs. 4 and 6, is expected to be caused by the increase of θ_{CO} above ~0.8. Under these conditions, Temkin isotherm can no longer be approximated by the logarithmic Eq. (6). At θ_{CO} exceeding ~0.8 growth of θ_{CO} with the increase of P_{CO} is slowed down compared to the trend expressed by Eq. (6) [73,74]. The negative order of CO oxidation rate in respect to P_{CO} is a long known phenomenon in heterogeneous catalysis [39]. It is caused by "CO inhibition", which consists in the decrease of a number of sites available for oxygen adsorption with the increase of CO coverage on the noble metal catalyst surface, Pt catalyst in particular, e.g. [39,75,76]. Negative fractional CO electrooxidation reaction order in respect to CO concentration in electrolyte was observed in acidic aqueous electrolytes on Pt [3] ($m \sim -0.6$) and Pt–Ru [38] ($m \sim -0.2$) at high CO coverage. Positive fractional values of m were observed in acidic aqueous electrolytes on Pt_3Sn single crystal electrode ($m = 0.25$–0.65) [77], on Pt–Ru ($m = 0.4$–1) [78] and on Pt–Ru in phosphotungstic acid ($m \sim 0.5$) [79].

The use of Pt–Ru in place of Pt results mainly in a shift of the CO electrooxidation voltammograms along potential axis by ~0.3 V in negative direction. In terms of Eq. (9b) the potential shift could be caused by the negative shift of the standard equilibrium potential E^0 of reaction (2) or by the increase of K value by a factor of ~2000. The shift of E^0 by approx. −0.3 V with the replacement Pt by Pt–Ru consents with the bifunctional mechanism of CO electrooxidation on Pt alloy catalysts. The similar (−0.25 V) shift of CO electrooxidation voltammetry curve with the replacement of Pt electrode with Pt–Ru was observed in aqueous H_2SO_4 [37,38]. In aqueous electrolytes Ru surface oxidation starts at ~0.2 V vs. RHE. This potential is about 0.4 V more negative than the potential of surface oxidation of Pt [41].

The results of the present study on CO electrooxidation kinetics can be compared with the results of our earlier study on CO tolerance of Pt and Pt–Ru hydrogen oxidation anodes of PEM FC with PBI–PA membranes [59]. In the practical regime of PEM FC operation, anode potential losses cannot exceed ~50 mV. In [59] at 180 °C Pt and Pt–Ru hydrogen oxidation catalysts were found nearly equal in CO tolerance. In particular, using (89% H_2–11% CO) gas mixture humidified to reach RH = 0.025, at 180 °C, hydrogen oxidation overvoltage at $i = 0.3\,A\,cm^{-2}$ on both Pt and Pt–Ru anodes was found ~20 mV (Figs. 3 and 4 [59]). This anode feed composition can be translated into the units of the component partial pressure used in this work ($P_{CO} = 0.083$ bar, $P_{H_2} = 0.667$ bar, $P_W = 0.25$ bar). The data of the present work enables to estimate the rate of the parallel process of CO electrooxidation, which could occur at the hydrogen oxidation anodes supplied with H_2–CO mixture in [59], provided that CO electrooxidation current at $E \sim 0.02$ V can be evaluated by extrapolation of the Tafel regions of the respective CO oxidation voltammetry curves. Extrapolation to $E = 0.02$ V of Tafel regions of CO electrooxidation curves, shown in Fig. 8(a) and (b) of this work, give CO oxidation current density at 180 °C, $P_{CO} = 0.07$ bar, $P_W = 0.25$ bar of the order of $10\,\mu A\,cm^{-2}$ on Pt–Ru, and $10\,nA\,cm^{-2}$ on Pt. Firstly, these extrapolated CO oxidation current density values differ by a factor of 1000, while Pt and Pt–Ru under the above indicated conditions were found nearly equal in CO tolerance. Secondly, the extrapolated CO oxidation currents at $P_{CO} = 0.07$ bar, Fig. 8(a) and (b), are smaller than current den-

sity of hydrogen oxidation in the presence of CO at the similar level ($E \approx 0.02$ V, $P_{CO} = 0.083$ bar, $i = 0.3$ A cm^{-2} [59]) approximately by a factor of 3×10^4 on Pt–Ru and 3×10^7 on Pt. It is hard to envision the way by which the very slow process of CO electrooxidation could control the rate of the very fast process of hydrogen electrooxidation. Thirdly, mass transport limitations of the CO electrooxidation, which apparently influence catalyst surface coverage by the adsorbed species, were observed in the present work at 180 °C, $P_{CO} = 0.048$ bar, when CO oxidation currents reached the level of ~0.3 A cm^{-2}, Fig. 3. This current density value is many orders of magnitude higher (by a factor of 3×10^4 on Pt–Ru and 3×10^7 on Pt) than the estimated rate of the parallel process of CO electrooxidation at the hydrogen oxidation anodes supplied with humidified 89% H_2–11% CO mixture [59]. Taking all that into account, we conclude that CO surface coverage on Pt or Pt–Ru hydrogen oxidation anodes studied in [59] was virtually unaffected by the parallel CO electrooxidation process. Therefore, CO electrooxidation can hardly play significant role in CO tolerance of Pt and Pt–Ru anodes of PEM FC with PBI–PA membranes in a practically important regime of operation.

The above proposed simplified mechanism of the CO electrooxidation on Pt and Pt–Ru anodes in PA at elevated temperature assumes that the rate of the process is controlled by the chemical reaction (3), that occurs entirely on Pt. Shift of the Pt electrode potential to more positive values results mainly in the increase of the surface coverage by the adsorbed active oxygen containing species. The replacement of Pt by Pt–Ru alloy at the electrode at fixed potential results in the increase of θ_{OH} on electrocatalyst surface by a factor of ~2000. In terms of the Pt catalyst surface coverage by OH_{ads} species, it is equivalent to 0.3 V shift of the Pt electrode potential. In view of the above considerations, the nearly numerical coincidence of the values of the apparent activation energy $E_{a\,app}$, measured with Pt and Pt–Ru electrocatalysts at potentials 0.7 V and 0.4 V, respectively, seems reasonable. If the above arguments are true, the current density measurements, used for evaluation of $E_{a\,app}$ on Pt and Pt–Ru, were performed at the same values of θ_{OH} and θ_{CO} on both catalysts at each particular temperature. The parity of the values of the apparent activation energy $E_{a\,app}$, measured with Pt and Pt–Ru, implies that kinetics of the rate limiting reaction (3) on Pt and Pt–Ru is essentially the same. The $E_{a\,app} = 110 \pm 15$ kJ mol^{-1}, determined in this work, is in reasonable agreement with the apparent activation energy value of CO electrooxidation on Pt in aqueous 0.5 M H_2SO_4 measured in the temperature domain 273–333 K – 132 kJ mol^{-1} in [35].

5. Conclusions

1) CO electrooxidation on Pt and Pt–Ru in phosphoric acid was studied by slow scan rate voltammetry in the temperature range 120–180 °C using MEA with PBI–PA membrane. The working electrode was supplied with gaseous CO–N_2–H_2O mixture of controlled composition. CO electrooxidation voltammetry curves on Pt and Pt–Ru were found to follow Tafel behavior with a slope of 80–100 mV per decade in a wide potential range. Influence of water vapor pressure and CO concentration in the anode feed gas on CO electrooxidation rate was studied. CO electrooxidation processes on Pt and Pt–Ru were found to follow the same trend. In terms of CO electrooxidation voltammetry, replacement of Pt by Pt–Ru resulted mainly in the shift of the curves in negative direction along potential axis by ~0.3 V. Reaction order in respect to P_W was found close to unity with both electrocatalysts. Reaction order in respect to P_{CO} was found negative, dependent on P_{CO}. At low P_{CO}, 0.002–0.03 bar, CO electrooxidation current both on Pt and Pt–Ru decreased linearly with the increase of $\log(P_{CO})$. The reaction order in respect to P_{CO} averaged over the whole P_{CO} range (0.95–0.0018 bar) was found $m \sim -0.01$ on both Pt and Pt–Ru. Measurements of the temperature dependence of CO electrooxidation rate revealed apparent activation energy of CO electrooxidation $E_{a\,app} = 110 \pm 15$ kJ mol^{-1} on both Pt and Pt–Ru. At low CO concentration $P_{CO} < 0.047$ bar and high water vapor pressure, CO electrooxidation was mass transport limited at high overvoltages.
2) The results were interpreted within the framework of Langmuir–Hinshelwood mechanism. To arrive at the equation, which describes the main features of CO electrooxidation, the following assumptions were made:
   a) Fast, reversible CO adsorption follows Temkin isotherm.
   b) Fast reversible electrochemical water oxidation with formation of adsorbed active oxygen containing species occurs at the unoccupied by CO catalyst sites only.
   c) The surface reaction between adsorbed CO and adsorbed active oxygen containing species, which produces $COOH_{ad}$, is the rate-determining stage.
   d) The fast irreversible electrochemical step of $COOH_{ad}$ oxidation doubles the current density value.

   The resulting Eq. (9b) is of the form of the Tafel equation with the slope value 2.303 RT/F. In contradistinction to the Tafel equation, E^0 in Eqs. (9a) and (9b) stands for the standard equilibrium potential of the one electron water oxidation reaction with formation of surface oxides, but not for the equilibrium potential of CO electrooxidation. Therefore, E^0 depends strongly on the nature of the catalyst metal. According to this approach, the main difference between CO electrooxidation processes on Pt and Pt–Ru is the disparity in E^0 values. In view of the above assumptions, parity of apparent activation energy $E_{a\,app}$ values, measured with Pt and Pt–Ru, implies that kinetics of the rate-determining reaction (3) on Pt and Pt–Ru is essentially the same.
3) Comparing the results of the present study with the results of our earlier work [59] on the CO tolerance of Pt and Pt–Ru it was concluded that CO electrooxidation can hardly play significant role in CO tolerance of Pt and Pt–Ru anodes of PEM FC with PBI–PA membranes supplied with hydrogen fuel containing CO at the level of few percent. Under these conditions the CO surface coverage on Pt or Pt–Ru hydrogen oxidation anodes cannot be altered by the very slow CO electrooxidation process.

Acknowledgement

The work was supported by the 3P Program of fundamental studies "Chemical Aspects of Power Generation" established by the Presidium of Russian Academy of Sciences.

References

[1] S. Ye, in: J. Zhang (Ed.), PEM Fuel Cell Electrocatalysts and Catalyst Layers. Fundamentals and Application, Springer–Verlag, London, 2008, Ch.16, pp. 759–834.
[2] S. Srinivasan, Fuel Cells From Fundamentals to Applications, Springer Science/Business Media, New York, 2006, Chapter 5, pp. 235–266.
[3] T.J. Schmidt, H.A. Gasteiger, R.J. Behm, J. Electrochem. Soc. 146 (1999) 1296–1304.
[4] M. Heinen, Z. Jusys, R.J. Behm, ECS Trans. 25 (1) (2009) 259–269.
[5] Q. Li, J.O. Jensen, R.F. Savinell, N.J. Bjerrum, Prog. Polym. Sci. 34 (2009) 449–477.
[6] Q. Li, R. He, J.O. Jensen, N.J. Bjerrum, Chem. Mater. 15 (2003) 4896–4915.
[7] O. Savadogo, J. Power Sources 127 (2004) 135–161.
[8] A.R. Korsgaard, R. Refshauge, M.P. Nielsen, M. Bang, S.K. Kær, J. Power Sources 162 (2006) 239–245.
[9] K. Kwon, D.Y. Yoo, J.O. Park, J. Power Sources 185 (2008) 202–206.
[10] T.J. Schmidt, in: F.N. Büchi, M. Inaba, T.J. Schmidt (Eds.), Polymer Electrolyte Fuel Cell Durability, Springer Science/Business Media, New York, 2009, pp. 199–221.
[11] J. Mader, L. Xiao, T.J. Schmidt, B.C. Benicewicz, Adv. Polym. Sci. 216 (2008) 63–124.
[12] C.-P. Wang, H.-S. Chu, Y.-Y. Yan, K.-L. Hsueh, J. Power Sources 170 (2007) 235–241.

[13] S.K. Das, A. Reis, K.J. Berry, J. Power Sources 193 (2009) 691–698.
[14] Q. Li, R. He, J.-A. Gao, J.O. Jensen, N.J. Bjerrum, J. Electrochem. Soc. 150 (2003) A1599–A1605.
[15] T.J. Schmidt, J. Baurmeister, ECS Trans. 16 (2) (2008) 263–270.
[16] J.-T. Wang, J.S. Wainright, R.F. Savinell, M. Litt, J. Appl. Electrochem. 26 (1996) 751–756.
[17] J. Lobato, P. Cañizares, M.A. Rodrigo, J.J. Linares, R. López-Vizcaíno, Energy Fuels 22 (2008) 3335–3345.
[18] J. Lobato, P. Cañizares, M.A. Rodrigo, J.J. Linares, Fuel Cells 9 (2009) 597–604.
[19] J. Wang, S. Wasmus, R.F. Savinell, J. Electrochem. Soc. 142 (1995) 4218–4224.
[20] M. Weber, J.-T. Wang, S. Wasmus, R.F. Savinell, J. Electrochem. Soc. 143 (1996) L158–L160.
[21] D.W. McKee, A.J. Scarpellino, Electrochem. Technol. 6 (1968) 101–105.
[22] L.W. Niedrach, D.W. McKee, J. Paynter, I.F. Danzig, Electrochem. Technol. 5 (1967) 318–323.
[23] M. Watanabe, S. Motoo, J. Electroanal. Chem. 60 (1975) 275–283.
[24] S. Gilman, J. Phys. Chem. 68 (1964) 70–80.
[25] S. Enbäck, G. Lindbergh, J. Electrochem. Soc. 152 (2005) A23–A31.
[26] C. Lu, C. Rice, R.I. Masel, P.K. Babu, P. Waszczuk, H.S. Kim, E. Oldfield, A. Wieckowski, J. Phys. Chem. B 106 (2002) 9581–9589.
[27] G.A. Camara, E.A. Ticianelli, S. Mukerjee, S.J. Lee, J. McBreen, J. Electrochem. Soc. 149 (2002) A748–A753.
[28] H.A. Gasteiger, N. Markovic, P.N. Ross, E.J. Cairns, J. Phys. Chem. 98 (1994) 617–625.
[29] B.E. Hayden, in: A. Wieckowski, E.R. Savinova, C.G. Vayenas (Eds.), Catalysis and Electrocatalysis at Nanoparticle Surfaces, Marcel Dekker, New York, 2003, Chapter 5, pp. 171–210.
[30] A.B. Anderson, E. Grantscharova, J. Phys. Chem. 99 (1995) 9143–9148.
[31] C.S. Lai, N.P. Lebedeva, T.H.M. Housmans, M.T.M. Koper, Top. Catal. 46 (2007) 320–333.
[32] Z. Jusys, J. Kaiser, R.J. Behm, Phys. Chem. Chem. Phys. 3 (2001) 4650–4660.
[33] T.T. Nwoga, J.W. Van Zee, Electrochem. Solid-State Lett. 11 (2008) B122–B126.
[34] G. Samjeské, K. Komatsu, M. Osawa, J. Phys. Chem. C 113 (2009) 10222–10228.
[35] E. Herrero, M. Feliu, Langmuir 16 (2000) 4779–4783.
[36] A.B. Anderson, N.M. Neshev, J. Electrochem. Soc. 149 (2002) E383–E388.
[37] H.A. Gasteiger, N. Marković, P.N. Ross Jr., E.J. Cairns, J. Phys. Chem. 98 (1994) 617–625.
[38] H.A. Gasteiger, N. Marković, P.N. Ross Jr., E.J. Cairns, J. Phys. Chem. 99 (1995) 16757–16767.
[39] I. Langmuir, Trans. Faraday Soc. 17 (1922) 621–654.
[40] M.T.M. Koper, Faraday Discuss. 140 (2008) 11–24.
[41] N.S. Marinkovic, M.B. Vukmirovic, R.R. Adzic, in: C. Vayenas, R. White, M. Gamboa-Adelco (Eds.), Modern Aspects of Electrochemistry, vol. 42, Springer, New York, 2008, pp. 1–52.
[42] P.N. Ross, K. Kinoshita, A.J. Scarpellino, P. Stonehart, J. Electroanal. Chem. 63 (1975) 97–110.
[43] M.P. Hogarth, T.R. Ralph, Platinum Met. Rev. 46 (2002) 117–135.
[44] F. Bautier de Mongeot, M. Scherer, B. Gleich, E. Kopatzki, R.J. Behm, Surf. Sci. 411 (1998) 249–262.
[45] H. Uchida, K. Izumi, M. Watanabe, J. Phys. Chem. B 110 (2006) 21924–21930.
[46] L. Giorgi, A. Pozio, C. Bracchini, R. Giorgi, S. Turtù, J. Appl. Electrochem. 31 (2001) 325–334.
[47] J.C. Davies, J. Bonde, Á. Logadóttir, J.K. Nørskov, I. Chorkendorff, Fuel Cells 5 (2005) 429–435.
[48] M.T.M. Koper, T.E. Shubina, R.A. van Santen, J. Phys. Chem. B 106 (2002) 686–692.
[49] S. Papadimitriou, S. Armyanov, E. Valova, A. Hubin, O. Steenhaut, E. Pavlidou, G. Kokkinidis, S. Sotiropoulo, J. Phys. Chem. C 114 (2010) 5217–5223.
[50] B. Du, R. Pollard, J.F. Elter, M. Ramani, in: F.N. Büchi, M. Inaba, T.J. Schmidt (Eds.), Polymer Electrolyte Fuel Cell Durability, Springer Science/Business Media, New York, 2009, pp. 341–368.
[51] C. He, H.R. Kunz, J.M. Fenton, J. Electrochem. Soc. 144 (1997) 970–979.
[52] R.F. Savinell, E. Yeager, D. Tryk, U. Landau, J. Wainright, D. Weng, K. Lux, M. Litt, C. Rogers, J. Electrochem. Soc. 141 (1994) L46–L48.
[53] J.S. Wainright, J.T. Wang, D. Weng, R.F. Savinell, M. Litt, J. Electrochem. Soc. 142 (1995) L121–L123.
[54] Y.-L. Ma, J.S. Wainright, M.H. Litt, R.F. Savinell, J. Electrochem. Soc. 151 (2004) A8–A16.
[55] R.P. Jayakody, S.H. Chung, L. Durantino, H. Zhang, C.L. Xiao, B.C. Benicewicz, S.G. Greenbaum, J. Electrochem. Soc. 154 (2007) B242–B246.
[56] C.E. Hughes, S. Haufe, B. Angerstein, R. Kalim, U. Mähr, A. Reiche, M. Baldus, J. Phys. Chem. B 108 (2004) 13626–13631.
[57] A. Schechter, R.F. Savinell, J.S. Wainright, D. Ray, J. Electrochem. Soc. 156 (2009) B283–B290.
[58] P. Stonehart, D. Wheeler, in: B.E. Conway, C.G. Vayenas, R.E. White, M.E. Gamboa-Adelco (Eds.), Modern Aspects of Electrochemistry, vol. 38, Kluwer Academic/Plenum Publishers, New York, 2005, pp. 373–424, Chapter 4.
[59] A.D. Modestov, M.R. Tarasevich, V.Ya. Filimonov, E.S. Davydova, Electrochim. Acta 55 (2010) 6073–6080.
[60] D.I. MacDonald, J.R. Boyack, J. Chem. Eng. Data 14 (1969) 380–384.
[61] B.J. Fontana, J. Am. Chem. Soc. 73 (1951) 3348–3350.
[62] A.D. Modestov, M.R. Tarasevich, V.Ya. Filimonov, A.Yu. Leykin, J. Electrochem. Soc. 156 (2009) B650–B656.
[63] A.D. Modestov, M.R. Tarasevich, V.Ya. Filimonov, N.M. Zagudaeva, Electrochim. Acta 54 (2009) 7121–7127.
[64] A.Y. Leykin, O.A. Shkrebko, M.R. Tarasevich, J. Membr. Sci. 328 (2009) 86–89.
[65] A.Y. Leykin, A.A. Askadskii, V.G. Vasilev, A.L. Rusanov, J. Membr. Sci. 347 (2010) 69–74.
[66] J.A. Dean (Ed.), Lange's Handbook of Chemistry, 15th edn, McGraw-Hill, Inc, 1999 (Section 5).
[67] D.D. Cheddie, N. Munroe, J. Power Sources 156 (2006) 414–423.
[68] R.N. Carter, T.A. Greszler, D.R. Baker, ECS Trans. 25 (1) (2009) 225–231.
[69] N.M. Marković, T.J. Schmidt, B.N. Grgur, H.A. Gasteiger, R.J. Behm, P.N. Ross, J. Phys. Chem. B 103 (1999) 8568–8577.
[70] G. Kohlmayr, P. Stonehart, Electrochim. Acta 18 (1973) 211–223.
[71] H.P. Dhar, L.G. Christner, A.K. Kush, J. Electrochem. Soc. 134 (1987) 3021–3026.
[72] H.P. Dhar, L.G. Christner, A.K. Kush, H.C. Maru, J. Electrochem. Soc. 133 (1986) 1574–1582.
[73] M.I. Temkin, Zh. Fiz. Khim. 15 (1941) 296–332.
[74] J.O'M. Bockris, A.K.N. Reddy, M. Gamboa-Aldeco, Modern Electrochemistry, vol. 2A, 2nd edn, Kluwer Academic Publishers, New York, 2000, Chapter 6, 938–1030.
[75] F. Gao, Y. Wang, Y. Cai, D.W. Goodman, J. Phys. Chem. C 113 (2009) 174–181.
[76] H.D. Lewis, D.J. Burnett, A.M. Gabelnick, D.A. Fischer, J.L. Glan, J. Phys. Chem. B 109 (2005) 21847–21857.
[77] H.A. Gasteiger, N.M. Markovic, P.N. Ross Jr., Catal. Lett. 36 (1996) 1–8.
[78] A.S. Aricó, E. Modica, I. Ferrara, E. Passalacqua, V. Antonucci, P.L. Antonucci, J. Appl. Electrochem. 27 (1997) 1275–1282.
[79] A.S. Aricó, E. Modica, I. Ferrara, V. Antonucci, J. Appl. Electrochem. 28 (1998) 881–887.